High-fold γ-ray spectroscopy of ^{117}I: Coexistence of collective and noncollective structures

E. S. Paul,[1] D. B. Fossan,[2] K. Hauschild,[3,*] I. M. Hibbert,[3,†] P. J. Nolan,[1] H. Schnare,[2,‡] J. M. Sears,[2] I. Thorslund,[2] R. Wadsworth,[2] A. N. Wilson,[1,§] J. N. Wilson,[1,‖] and I. Ragnarsson[4]

[1]*Oliver Lodge Laboratory, University of Liverpool, P.O. Box 147, Liverpool L69 7ZE, United Kingdom*

[2]*Department of Physics and Astronomy, State University of New York at Stony Brook, Stony Brook, New York 11794*

[3]*Department of Physics, University of York, Heslington, York YO1 5DD, United Kingdom*

[4]*Department of Mathematical Physics, University of Lund, P.O. Box 118, S-22100 Lund, Sweden*

(Received 3 December 1998)

High-spin states have been populated in $^{117}_{53}$I via the ^{90}Zr(^{31}P,$2p2n$) reaction at 150 MeV, using the EUROGAM II γ-ray spectrometer to record high-fold γ-ray coincidences. A quadruples γ-ray analysis (γ^4) has been used to extend the known level scheme. In addition to several aligned noncollective states, a new high-spin band showing characteristics of smooth termination has been established at and linked into the low-spin level scheme. Its structure has been inferred through comparison with cranked Nilsson-Strutinsky calculations. [S0556-2813(99)03804-2]

PACS number(s): 27.60.+j, 23.20.Lv, 21.10.Re, 25.70.Gh

I. INTRODUCTION

The neutron-deficient iodine ($Z=53$) isotopes contain sufficient valence particles outside of the $Z=N=50$ doubly closed core to induce low-spin collectivity (i.e., quadrupole deformation, $\varepsilon_2>0$). However, the underlying softness with respect to γ, the triaxiality coordinate in the polar representation of rotating quadrupole shapes, allows deviations away from (prolate, $\gamma=0°$) axial symmetry. Moreover, the valence particles can only generate a finite spin leading to the observation of energetically favored noncollective oblate ($\gamma=60°$) states that compete with the collective prolate configurations. Such states at $I^\pi=39/2^-$ and $I^\pi=43/2^-$ have been systematically observed in the series of odd-A iodine isotopes from $A=115$ to $A=123$ [1–5] and correspond to states where the nuclear spin is generated entirely from the single-particle angular momenta of the valence particles. These specific states at $I\sim 20\hbar$ do not represent the maximal alignment of all the valence particles, which can accommodate $30-40\hbar$; such maximally aligned states represent so-called band termination states for a given configuration.

Low-spin collectivity in this mass region can also be induced by particle-hole (p-h) excitations across the $Z=50$ shell gap. For example, 1p-1h excitations involving the $\pi g_{9/2}^{-1}$ orbital lead to strongly coupled $\Delta I=1$ bands in these nuclei [6]. Furthermore, 2p-2h excitations involving the $\pi g_{9/2}^{-2}$ configuration are also possible, e.g., 0_2^+ states in even tin isotopes [7]. These particle-hole excitations are of particular interest since they can further enhance the quadrupole deformation of the nucleus, while augmenting the available spin before band termination is achieved ($I\sim 40-50\hbar$). Indeed, such configurations have led to the observation of ''smooth terminating bands'' [8] in this mass region which consist of long sequences of γ-ray transitions. Theoretically, these structures represent a slow drift of the nuclear shape from prolate to oblate over many units of spin [9]. The gradual loss of collectivity, associated with this slow drift through the $\varepsilon_2-\gamma$ plane, has been experimentally verified through recent lifetime measurements of states in smooth terminating bands of ^{108}Sn and ^{109}Sb [10].

Although evidence for specific noncollective oblate states in ^{117}I had been found prior to the present investigation [2], there was no evidence for smooth terminating bands in this nucleus, although several were known in ^{113,115}I [11,12]. New data have however uncovered a single band in ^{117}I showing properties of smooth termination at high spin; this band has been connected into the low-spin level structure thus allowing an estimate of the spin, parity and excitation energy of the band (note that the majority of smooth terminating bands remain unlinked into the low-spin level schemes). Cranked Nilsson-Strutinsky calculations [13,14] have been used to determine possible single-particle configurations for this band. The present paper documents the new results for ^{117}I obtained with the EUROGAM II γ-ray spectrometer. A quadruples (γ^4) analysis of the data has been undertaken using the recently available RADWARE 4D ''hypercube'' software. Previous experimental work on high-spin states in this nucleus may be found in Refs. [2,15–19].

II. EXPERIMENTAL DETAILS

High-spin states in ^{117}I were populated using the ^{90}Zr(^{31}P,$2p2n$) fusion-evaporation reaction, performed at the Center de Recherches Nucléaires, Strasbourg. The Vivitron electrostatic accelerator provided a 150 MeV ^{31}P beam which bombarded two stacked self-supporting target foils of

*Present address: Lawrence Livermore National Laboratory, P.O. Box 808, L-280, Livermore, CA 94550.

†Present address: Oliver Lodge Laboratory, University of Liverpool, P.O. Box 147, Liverpool L69 7ZE, United Kingdom.

‡Present address: Institut für Kern- und Teilchenphysik, TU Dresden, Mommsenstr. 13, D-01062 Dresden, Germany.

§Present address: Department of Physics, University of York, Heslington, York YO1 5DD, United Kingdom.

‖Present address: Department of Chemistry, Washington University, St. Louis, MO 63130.

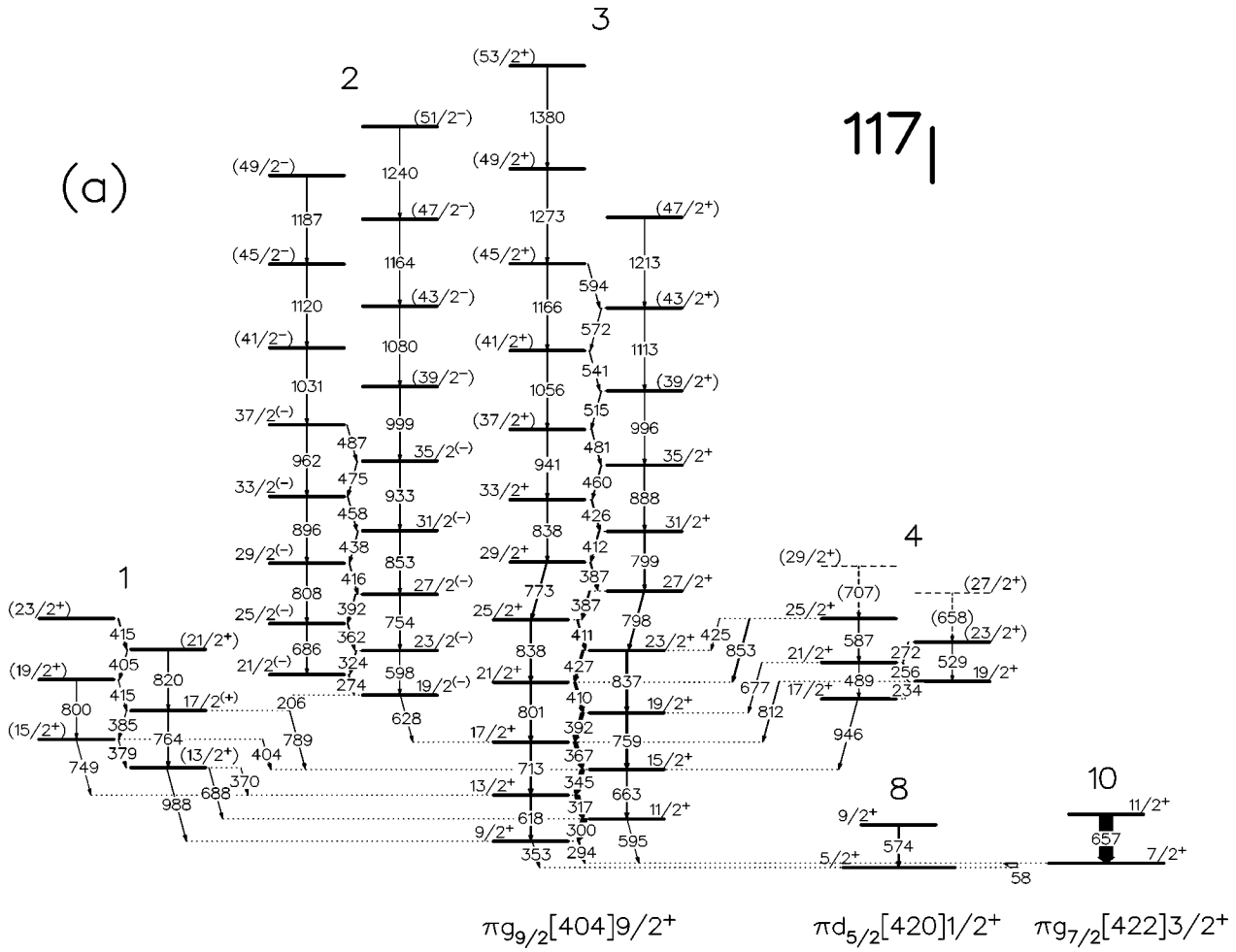

FIG. 1. Level scheme deduced for ^{117}I from this work. The transition energies are given in keV and their relative intensities are proportional to the widths of the arrows.

^{90}Zr (>97% enriched), each of nominal thickness 440 μg/cm^2. Coincident escape-suppressed, high-fold γ-ray events (γ^n, $n \geq 5$), within a prompt time window of 50 ns, were collected using the EUROGAM II spectrometer [20]. Approximately 8.5×10^8 such events were accumulated in 48 hours of beam time.

The EUROGAM II spectrometer contained the full complement of 54 Compton-suppressed HPGe detectors, including 24 segmented (four-element ''clover'' detectors [21], for this experiment. Energy and efficiency calibrations of the HPGe detectors were achieved using standard ^{133}Ba and ^{152}Eu radioactive sources placed at the target position. In addition to ^{117}I, many other reaction channels were also populated with significant strength, namely the $^{116-118}_{54}$Xe, $^{115,116,118}_{53}$I, $^{114-117}_{52}$Te and $^{112-114}_{51}$Sb nuclides. Results for several of these nuclei from this data set have previously been published in Refs. [22–26].

III. RESULTS

A. Level scheme construction

In order to investigate the level scheme of ^{117}I, the high-fold data were unfolded off-line into constituent quadruple (γ^4) coincidence events, software gain matched, and replayed into a RADWARE 4D hypercube with a nonlinear gain compression of 2.2 channels/FWHM [27]. In this way, γ-rays with energies between 50 keV and 2.5 MeV were stored in the hypercube which had 1023 channels per dimension. Approximately 17 quadruples per event were found leading to a total of 1.5×10^{10} events incremented into the hypercube, which required 6.0 Gbytes of disk space for storage. Analysis of the hypercube was conducted using the 4DG8R graphical analysis package, an extension of the 3D LEVIT8R software [27] to four dimensions.

The deduced level scheme of ^{117}I is shown in Fig. 1, where the ordering of transitions is based on relative γ-ray intensities and quadruple (γ^4) coincidence relationships. The γ-rays have been arranged into several band structures, labeled 1–14. A complete 4D analysis is necessarily complex and time consuming. The RADWARE analysis package however allows one to readily set γ-ray gates (or a list of gates) on three axes of the hypercube (x, y, z axes) and project out ''triple-gated'' 1D spectra onto the fourth dimension (w axis). Examples of such triple-gated coincidence spectra are presented in Fig. 2 for some of the bands shown in Fig. 1. Several 1D spectra were also generated by directly unfolding the high-fold data under certain gating conditions, typically three or four simultaneous gates from a list of transitions. The unfolding procedure of Ref. [28] was used. An example of such a spectrum is shown in Fig. 3 for bands 9 and 10.

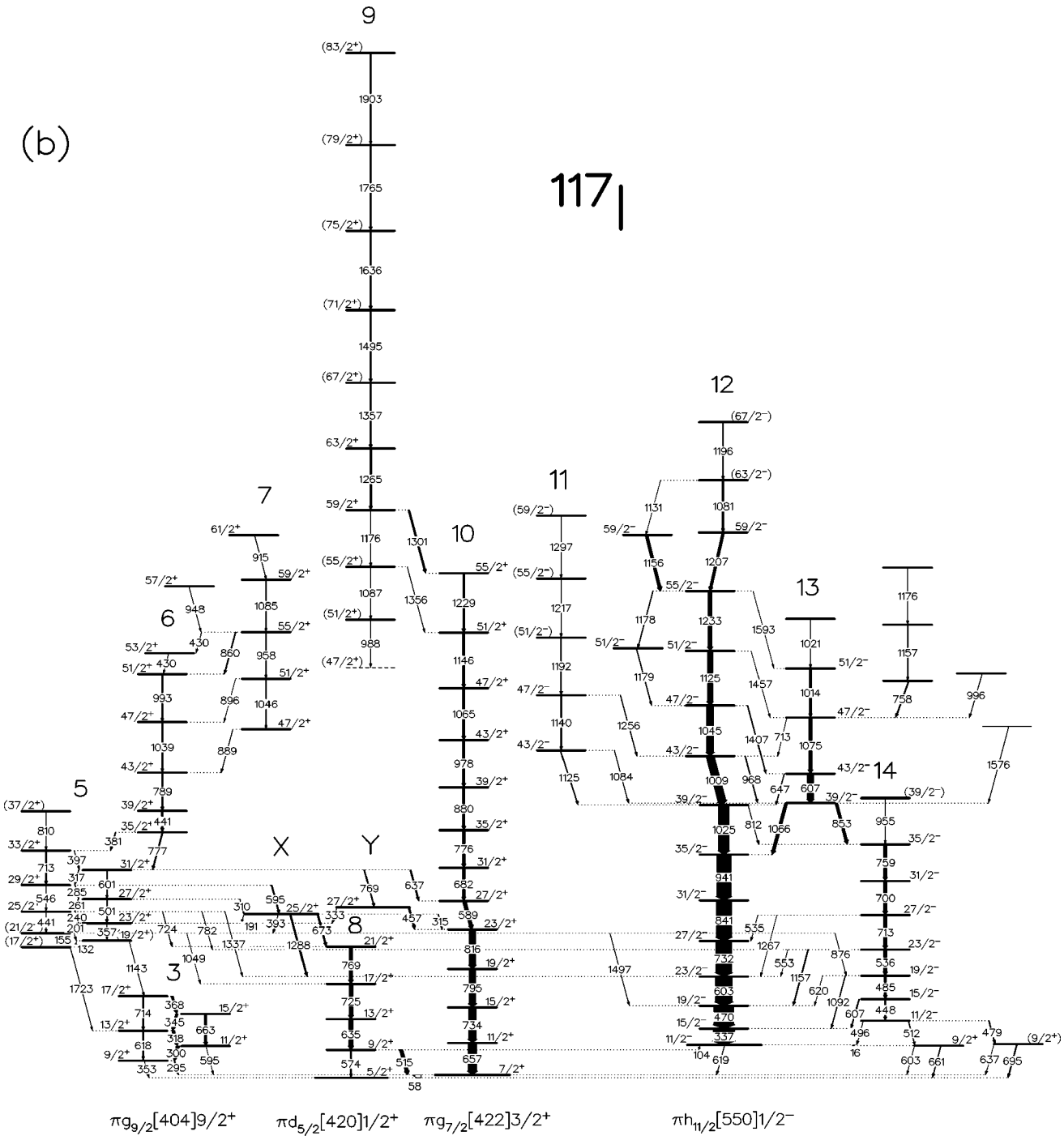

FIG. 1 (*Continued*).

The measured transition energies and the relative intensities of the ^{117}I γ-rays are listed in Table I. Given the complex nature of the deduced level scheme, in particular the occurrence of several self-coincident doublet (and triplet) transitions in addition to the weak intensity of many transitions, the precise determination of γ-ray energies and intensities was a difficult task. Indeed, more than 250 transitions have been placed in the level scheme. The measured transition energies and relative intensities of Table I were obtained by two methods: (i) multidimensional fits using the RADWARE codes, which work well for strong transitions ($I_\gamma > 10\%$ of the channel strength); and (ii) measurement of the energies and intensities in 1D spectra produced under certain (multiple) gating conditions. The latter method involved the generation of many 1D spectra. The γ-rays listed in Table I have been ordered by specific bands and each section contains the inband and depopulating transitions associated with the respective bands.

B. Spin and parity assignments

Multipolarities (L) for the majority of the transitions assigned to ^{117}I were determined from the data using the method of directional correlation of oriented states (DCO) [29]. Events recorded in the 24 ''central'' clover detectors near 90°, with respect to the beam direction, were sorted

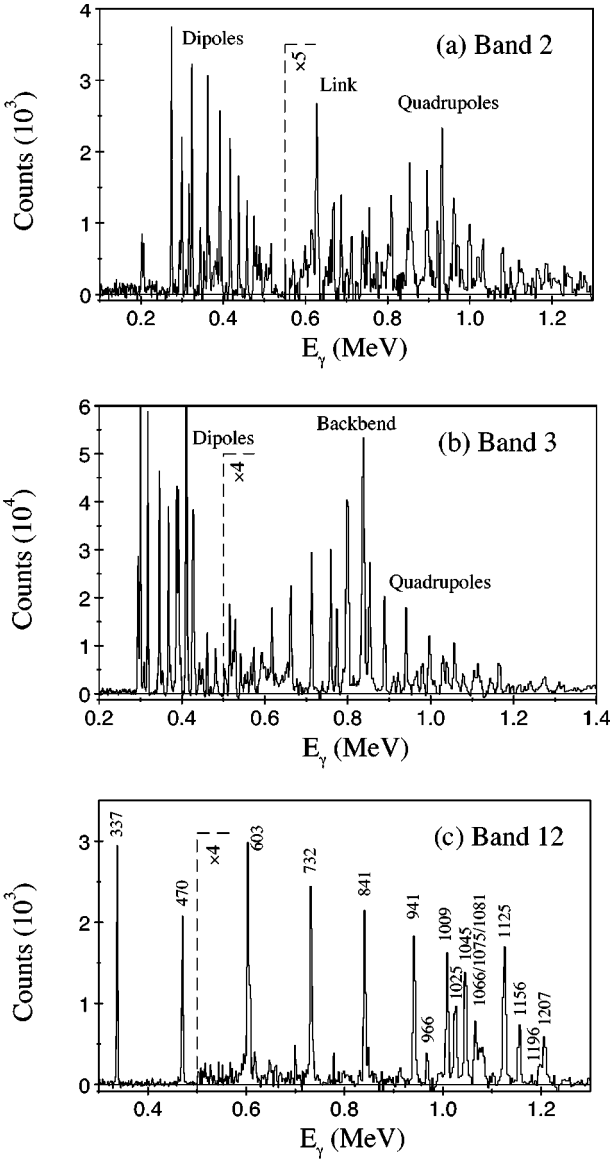

FIG. 2. Examples of triple-gated quadruple coincidence spectra with transition energies labeled in keV. Each spectrum was projected onto the *w* axis of the hypercube after lists of energies (gates) had been set on the *x*, *y*, and *z* axes, respectively. (a) Spectrum for band 2 ($x=y=z=$ all dipoles 206–511 keV). The 628 keV link into band 3 is labeled; (b) spectrum for band 3 ($x=y=z=$ all dipoles 300–515 keV). Excess intensity of the quadrupoles around 800 keV is due to overlapping doublet transitions associated with a backbend. (c) Spectrum for band 12 ($x=y=603$, 732, 841, 941, 1025 keV, $z=1233$ keV).

against those collected in the ''extreme'' forward and backward detectors (5 at 22.4° plus 5 at 157.6°) into a 2D matrix. An average DCO ratio was then obtained from measured γ-ray intensities I_γ as

$$R_{Q,D}=\frac{I_\gamma(\text{measured extreme, gated central})}{I_\gamma(\text{measured central, gated extreme})}, \qquad (1)$$

where the labels Q and D refer to the multipolarity of the gating transitions (quadrupole or dipole). Transitions of stretched-quadrupole character ($L=2$, $\Delta I=2$) were identified by R_Q values of approximately 1.0, although pure non-

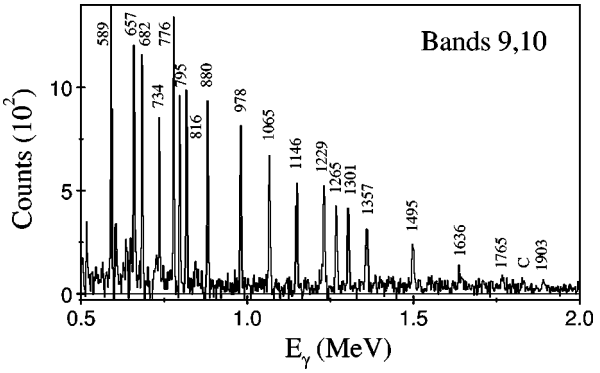

FIG. 3. Triple-gated coincidence spectrum for bands 9 and 10 unfolded directly from the high-fold data. Transition energies are labelled in keV, while ''C'' represents a contaminant.

stretched dipole ($L=1$, $\Delta I=0$) transitions are also expected to possess similar ratios. For the present geometry, R_Q values of approximately 0.55 are predicted for transitions of pure stretched-dipole character ($L=1$, $\Delta I=1$), using the formalism of Ref. [29]. Since a large part of the level scheme [Fig. 1(a)] consists of strongly coupled bands with strong dipole and weak quadrupole transitions, it was not possible to always gate on quadrupole transitions; hence R_D values were evaluated by gating on the strong dipole transitions. In this case, R_D values of approximately 1.5 are expected for a stretched quadrupole and 1.0 for a stretched dipole. As a consistency check, R_Q and R_D values were measured for strong known stretched $E2$ and $E1$ transitions in ^{117}I and neighboring nuclei produced in this experiment. The measured R_Q and R_D values for the transitions assigned to ^{117}I are included in Table I.

Multipolarity assignments may be further corroborated by extracting γ-ray linear polarizations in order to distinguish between electric (EL) and magnetic (ML) character. This can be achieved by considering the 24 four-element clover detectors of the EUROGAM II spectrometer as Compton polarimeters [21]. Two 2D matrices were constructed from the coincidence data (unfolding the events into constituent γ^2 doubles) corresponding to single hits in any detector (coaxial or clover) on one axis against clover double-hit scattering events on the second axis. The scattering events are defined as either perpendicular to the reaction plane (first matrix) or parallel to the reaction plane (second matrix). The number of perpendicular $N_\perp$ and parallel $N_\parallel$ scatters for a given γ-ray could be obtained by projecting out spectra gated by specific ^{117}I transitions on the single-hit axis of the respective matrix. Assuming that all 96 separate clover crystals have equal efficiencies, an experimental linear polarization can be defined as

$$P=\frac{1}{Q}\frac{N_\perp-N_\parallel}{N_\perp+N_\parallel}, \qquad (2)$$

where the measured polarization sensitivity Q for the clover detectors, a function of the γ-ray energy, is taken from Ref. [21].

Figure 4 shows the difference between two spectra, corresponding to clover perpendicular scatters and parallel scatters, respectively. These spectra were projected out of the

TABLE I. Measured properties of the γ-ray transitions assigned to ^{117}I.

Bands 1, 2						
E_γ (keV) [a]	I_γ [b]	R_D	P	Mult.	Assignment	Band
206.1	0.4	1.19(9)		dipole	$19/2^{(-)}\rightarrow 17/2$	$2\rightarrow 1$
274.0	3.0	0.92(4)	−0.24(25)	$M1/E2$	$21/2^{(-)}\rightarrow 19/2^{(-)}$	2
323.9	2.9	1.03(3)	−0.41(10)	$M1/E2$	$23/2^{(-)}\rightarrow 21/2^{(-)}$	2
362.1	2.7	1.08(5)	−0.21(11)	$M1/E2$	$25/2^{(-)}\rightarrow 23/2^{(-)}$	2
370.4	<1				$(13/2^+)\rightarrow 13/2^+$	$1\rightarrow 3$
379.1	<1				$(15/2^+\rightarrow 13/2^+)$	1
384.9	<1				$(17/2^+\rightarrow 15/2^+)$	1
392.3	2.6	1.02(3)	−0.13(11)	$M1/E2$	$27/2^{(-)}\rightarrow 25/2^{(-)}$	2
404	<1				$(15/2^+)\rightarrow 15/2^+$	$1\rightarrow 3$
404.5	<1				$(21/2^+\rightarrow 19/2^+)$	1
415	<1				$(19/2^+\rightarrow 17/2^+)$	1
415	<1				$(23/2^+\rightarrow 21/2^+)$	1
416.2	2.4	1.01(3)	−0.17(11)	$M1/E2$	$29/2^{(-)}\rightarrow 27/2^{(-)}$	2
437.6	2.2	1.09(5)	−0.19(14)	$M1/E2$	$31/2^{(-)}\rightarrow 29/2^{(-)}$	2
457.9	2.0	1.07(5)		$M1/E2$	$33/2^{(-)}\rightarrow 31/2^{(-)}$	2
474.8	1.7				$35/2^{(-)}\rightarrow 33/2^{(-)}$	2
486.7	1.1				$37/2^{(-)}\rightarrow 35/2^{(-)}$	2
598	0.2				$23/2^{(-)}\rightarrow 19/2^{(-)}$	2
627.7	0.6	0.97(4)	0.01(16)	$(E1)$	$19/2^{(-)}\rightarrow 17/2^+$	$2\rightarrow 3$
686.1	0.7				$25/2^{(-)}\rightarrow 21/2^{(-)}$	2
687.7	0.8				$(13/2^+)\rightarrow 11/2^+$	$1\rightarrow 3$
749	<1				$(15/2^+)\rightarrow 13/2^+$	$1\rightarrow 3$
754.3	1.8				$27/2^{(-)}\rightarrow 23/2^{(-)}$	2
764	<1				$17/2^{(+)}\rightarrow (13/2^+)$	1
789	<1				$17/2^{(+)}\rightarrow 15/2^+$	$1\rightarrow 3$
800	<1				$19/2^+\rightarrow 15/2^+$	1
808	1.2	1.21(7)		$E2$	$29/2^{(-)}\rightarrow 25/2^{(-)}$	2
820	<1				$(21/2^+)\rightarrow 17/2^{(+)}$	1
853	1.8	1.41(8)		$E2$	$31/2^{(-)}\rightarrow 27/2^{(-)}$	2
896	2.1				$33/2^{(-)}\rightarrow 29/2^{(-)}$	2
932.6	1.8	1.31(8)		$E2$	$35/2^{(-)}\rightarrow 31/2^{(-)}$	2
961.9	2.0	1.63(13)		$E2$	$37/2^{(-)}\rightarrow 33/2^{(-)}$	2
988	<1				$(13/2^+)\rightarrow 9/2^+$	$1\rightarrow 3$
998.9	1.6				$(39/2^-)\rightarrow 35/2^{(-)}$	2
1031.3	1.5				$(41/2^-)\rightarrow 37/2^{(-)}$	2
1079.6	1.4				$(43/2^-\rightarrow 39/2^-)$	2
1119.8	1.2				$(45/2^-\rightarrow 41/2^-)$	2
1164.2	1.0				$(47/2^-\rightarrow 43/2^-)$	2
1187.2	<1				$(49/2^-\rightarrow 45/2^-)$	2
1240.1	<1				$(51/2^-\rightarrow 47/2^-)$	2

Bands 3–4						
E_γ (keV) [a]	I_γ [b]	R_D	P	Mult.	Assignment	Band
233.6	1.0				$19/2^+\rightarrow 17/2^+$	4
256.2	3.1	0.96(5)		$M1/E2$	$21/2^+\rightarrow 19/2^+$	4
272.4	2.5				$(23/2^+)\rightarrow 21/2^+$	4
293.9	5	0.99(2)	−0.18(5)	$M1/E2$	$9/2^+\rightarrow 7/2^+$	$3\rightarrow 10$
299.8	23	0.98(2)	−0.26(5)	$M1/E2$	$11/2^+\rightarrow 9/2^+$	3
317.3	18	0.95(2)	−0.23(4)	$M1/E2$	$13/2^+\rightarrow 11/2^+$	3
345.1	16	1.03(2)	−0.23(4)	$M1/E2$	$15/2^+\rightarrow 13/2^+$	3
353.1	0.5				$9/2^+\rightarrow 5/2^+$	$3\rightarrow 8$
367.4	14	1.02(2)	−0.27(5)	$M1/E2$	$17/2^+\rightarrow 15/2^+$	3
386.6	12 [c]	0.94(3) [c]		$M1/E2$	$27/2^+\rightarrow 25/2^+$	3

TABLE I. (*Continued.*)

E_γ (keV) [a]	I_γ [b]	R_D	P	Mult.	Assignment	Band
386.6	12 [c]	0.94(3) [c]		$M1/E2$	$29/2^+ \rightarrow 27/2^+$	3
391.9	13	0.94(3)	–0.35(4)	$M1/E2$	$19/2^+ \rightarrow 17/2^+$	3
410.2	14 [c]	0.95(3) [c]	–0.19(3) [c]	$M1/E2$	$21/2^+ \rightarrow 19/2^+$	3
411	14 [c]	0.95(3) [c]	–0.19(3) [c]	$M1/E2$	$25/2^+ \rightarrow 23/2^+$	3
412	14 [c]	0.95(3) [c]	–0.19(3) [c]	$M1/E2$	$31/2^+ \rightarrow 29/2^+$	3
425	13 [c]	0.98(2) [c]	–0.19(3) [c]	$M1/E2$	$25/2^+ \rightarrow 23/2^+$	4→3
426	13 [c]	0.98(2) [c]	–0.29(5) [c]	$M1/E2$	$33/2^+ \rightarrow 31/2^+$	3
427	13 [c]	0.98(2) [c]	–0.29(5) [c]	$M1/E2$	$23/2^+ \rightarrow 21/2^+$	3
460.3	2.9	0.99(4)		$M1/E2$	$35/2^+ \rightarrow 33/2^+$	3
480.5	2.6				$(37/2^+) \rightarrow 35/2^+$	3
489.3	<1				$21/2^+ \rightarrow 17/2^+$	4
515.0	1.9				$(39/2^+ \rightarrow 37/2^+)$	3
529	<1				$(23/2^+) \rightarrow 19/2^+$	4
540.5	1.5				$(41/2^+ \rightarrow 39/2^+)$	3
572	<1				$(43/2^+ \rightarrow 41/2^+)$	3
586.6	1.4				$25/2^+ \rightarrow 21/2^+$	4
594	<1				$(45/2^+ \rightarrow 43/2^+)$	3
595.0	0.2				$11/2^+ \rightarrow 7/2^+$	3→10
617.5	4.0				$13/2^+ \rightarrow 9/2^+$	3
658	<1				$(27/2^+ \rightarrow 23/2^+)$	4
662.5	4.3	1.39(6)	0.46(12)	$E2$	$15/2^+ \rightarrow 11/2^+$	3
677.4	1.1	0.86(9)		$M1/E2$	$21/2^+ \rightarrow 19/2^+$	4→3
707	<1				$(29/2^+) \rightarrow 25/2^+$	4
712.5	6.4				$17/2^+ \rightarrow 13/2^+$	3
758.8	6.1	1.36(6)		$E2$	$19/2^+ \rightarrow 15/2^+$	3
773.9	4.0				$29/2^+ \rightarrow 25/2^+$	3
797	10 [c]				$27/2^+ \rightarrow 23/2^+$	3
799	10 [c]				$31/2^+ \rightarrow 27/2^+$	3
801	10 [c]				$21/2^+ \rightarrow 17/2^+$	3
811.7	2.0				$19/2^+ \rightarrow 17/2^+$	4→3
837	15 [c]	1.28(7) [c]		$E2$	$23/2^+ \rightarrow 19/2^+$	3
838	15 [c]	1.28(7) [c]		$E2$	$25/2^+ \rightarrow 21/2^+$	3
838	15 [c]	1.28(7) [c]		$E2$	$33/2^+ \rightarrow 29/2^+$	3
852.6	4.1	1.27(8)		$E2$	$25/2^+ \rightarrow 21/2^+$	4→3
888.1	2.1				$35/2^+ \rightarrow 31/2^+$	3
940.9	2.1				$(37/2^+) \rightarrow 33/2^+$	3
946.0	1.1	0.87(9)		$M1/E2$	$17/2^+ \rightarrow 15/2^+$	4→3
996.1	1.8				$(39/2^+) \rightarrow 35/2^+$	3
1056.1	2.0				$(41/2^+ \rightarrow 37/2^+)$	3
1113	1.4				$(43/2^+ \rightarrow 39/2^+)$	3
1166	1.6				$(45/2^+ \rightarrow 41/2^+)$	3
1213	1.0				$(47/2^+ \rightarrow 43/2^+)$	3
1273	1.4				$(49/2^+ \rightarrow 45/2^+)$	3
1380	1.0				$(53/2^+ \rightarrow 49/2^+)$	3

Bands 5–7

E_γ (keV) [a]	I_γ [b]	R_Q	P	Mult.	Assignment	Band
132.3	<1				$(19/2^+ \rightarrow 17/2^+)$	5
154.9	<1				$(21/2^+ \rightarrow 19/2^+)$	5
191.3	0.7				$25/2^+ \rightarrow 23/2^+$	X →5
200.9	1.0				$23/2^+ \rightarrow (21/2^+)$	5
240.3	1.2	0.48(4)		$M1/E2$	$25/2^+ \rightarrow 23/2^+$	5
260.6	3.5	0.55(4)	0.04(15)	$M1/E2$	$27/2^+ \rightarrow 25/2^+$	5
285.0	2.1	0.42(2)	–0.01(15)	$M1/E2$	$29/2^+ \rightarrow 27/2^+$	5

TABLE I (*Continued.*)

E_γ (keV) [a]	I_γ [b]	R_D	P	Mult.	Assignment	Band
309.6	2.2	0.63(2)	0.04(9)	$M1/E2$	$27/2^+ \rightarrow 25/2^+$	$5 \rightarrow$ X
315.0	3.4	0.85(9)		$M1/E2$	$25/2^+ \rightarrow 23/2^+$	X $\rightarrow 10$
316.5	3.1	0.51(3)	–0.28(12)	$M1/E2$	$31/2^+ \rightarrow 29/2^+$	5
333.0	1.0				$27/2^+ \rightarrow 23/2^+$	Y $\rightarrow 5$
356.6	0.3				$23/2^+ \rightarrow (19/2^+)$	5
380.5	4.5	0.70(6)	0.03(13)	$M1/E2$	$35/2^+ \rightarrow 33/2^+$	$6 \rightarrow 5$
392.8	1.1	1.02(3)		$E2$	$25/2^+ \rightarrow 21/2^+$	X $\rightarrow 5$
397.3	1.6	0.66(7)	–0.09(14)	$M1/E2$	$33/2^+ \rightarrow 31/2^+$	5
430.3	1.0 [c]	0.51(3) [c]	–0.01(7) [c]	$M1/E2$	$53/2^+ \rightarrow 51/2^+$	6
430.3	1.0 [c]	0.51(3) [c]	–0.01(7) [c]	$M1/E2$	$55/2^+ \rightarrow 53/2^+$	$7 \rightarrow 6$
440.9	9.5	1.03(4)	0.40(8)	$E2$	$39/2^+ \rightarrow 35/2^+$	6
441.0	2.6				$25/2^+ \rightarrow (21/2^+)$	5
456.7	10	1.19(5)		$E2$	$27/2^+ \rightarrow 23/2^+$	Y $\rightarrow 10$
501.4	4.9	1.21(9)		$E2$	$27/2^+ \rightarrow 23/2^+$	5
545.9	0.6				$29/2^+ \rightarrow 25/2^+$	5
594.9	6.8	0.95(5)		$E2$	$29/2^+ \rightarrow 25/2^+$	$5 \rightarrow$ X
600.9	2.6	1.12(7)	0.40(10)	$E2$	$31/2^+ \rightarrow 27/2^+$	5
636.8	8.0	0.99(4)	0.58(12)	$E2$	$31/2^+ \rightarrow 27/2^+$	$5 \rightarrow 10$
673.1	8.9	0.96(5)		$E2$	$25/2^+ \rightarrow 21/2^+$	X $\rightarrow 8$
712.9	6.9	1.10(8)		$E2$	$33/2^+ \rightarrow 29/2^+$	5
723.8	3.0				$25/2^+ \rightarrow 21/2^+$	$5 \rightarrow 8$
768.6	5.1	1.00(3)		$E2$	$31/2^+ \rightarrow 27/2^+$	$5 \rightarrow$ Y
777.2	6.5	0.99(4)	0.18(10)	$E2$	$35/2^+ \rightarrow 31/2^+$	$6 \rightarrow 5$
782.4	<1				$25/2^+ \rightarrow 23/2^-$	$5 \rightarrow 14$
788.9	8.7	1.00(3)	0.41(7)	$E2$	$43/2^+ \rightarrow 39/2^+$	6
810	<1				$(37/2^+) \rightarrow 33/2^+$	5
860.2	5.0	1.18(7)	0.38(9)	$E2$	$55/2^+ \rightarrow 51/2^+$	$7 \rightarrow 6$
876.2	<1				$(21/2^+) \rightarrow 19/2^-$	$5 \rightarrow 14$
888.5	1.4	0.97(4)	0.19(8)	$E2$	$47/2^+ \rightarrow 43/2^+$	$7 \rightarrow 6$
896.3	<1				$51/2^+ \rightarrow 47/2^+$	$7 \rightarrow 6$
915.4	1.5	0.21(2)	–0.15(8)	$M1/E2$	$61/2^+ \rightarrow 59/2^+$	7
948.1	0.8	0.26(2)	–0.34(10)	$M1/E2$	$57/2^+ \rightarrow 55/2^+$	$\rightarrow 7$
958.0	2.9	0.95(5)	0.64(17)	$E2$	$55/2^+ \rightarrow 51/2^+$	7
992.6	5.3	0.97(4)	0.17(8)	$E2$	$51/2^+ \rightarrow 47/2^+$	6
1038.5	5.4	1.12(4)	0.47(16)	$E2$	$47/2^+ \rightarrow 43/2^+$	6
1045.5	2.0	0.99(4)	0.19(21)	$E2$	$51/2^+ \rightarrow 47/2^+$	7
1048.7	<1				$(21/2^+) \rightarrow 17/2^+$	$5 \rightarrow 8$
1084.7	2.0	1.05(5)	0.34(8)	$E2$	$59/2^+ \rightarrow 55/2^+$	7
1142.7	<1				$(19/2^+) \rightarrow 17/2^+$	$5 \rightarrow 3$
1288.3	8.4	0.71(3)	0.21(12)	$E1$	$25/2^+ \rightarrow 23/2^-$	X $\rightarrow 12$
1337.1	<1				$25/2^+ \rightarrow 23/2^-$	$5 \rightarrow 12$
1497.1	1.0				$(21/2^+) \rightarrow 19/2^-$	$5 \rightarrow 12$
1723	<1				$(17/2^+) \rightarrow 13/2^+$	$5 \rightarrow 3$

Bands 8–10

E_γ (keV) [a]	I_γ [b]	R_Q	P	Mult.	Assignment	Band
58.3		1.66(8)		$M1/E2$	$7/2^+ \rightarrow 5/2^+$	$10 \rightarrow 8$
514.6	20	0.52(2)	–0.14(4)	$M1/E2$	$9/2^+ \rightarrow 7/2^+$	$8 \rightarrow 10$
573.5	5	0.97(5)		$E2$	$9/2^+ \rightarrow 5/2^+$	8
588.8	20	1.12(3)	0.24(6)	$E2$	$27/2^+ \rightarrow 23/2^+$	10
634.7	25	0.95(4)	0.49(7)	$E2$	$13/2^+ \rightarrow 9/2^+$	8
657.1	52	1.19(3)	0.42(10)	$E2$	$11/2^+ \rightarrow 7/2^+$	10
682.1	13	1.13(3)	0.31(9)	$E2$	$31/2^+ \rightarrow 27/2^+$	10
725.4	22	1.03(5)	0.31(8)	$E2$	$17/2^+ \rightarrow 13/2^+$	8

TABLE I (*Continued.*)

E_γ (keV) [a]	I_γ [b]	R_D	P	Mult.	Assignment	Band
733.5	45	1.01(2)	0.47(7)	$E2$	$15/2^+ \rightarrow 11/2^+$	10
768.7	20	0.94(5)	0.29(10)	$E2$	$21/2^+ \rightarrow 17/2^+$	8
775.7	13	1.13(4)	0.12(7)	$E2$	$35/2^+ \rightarrow 31/2^+$	10
795.0	40	1.06(2)	0.26(6)	$E2$	$19/2^+ \rightarrow 15/2^+$	10
815.5	37	0.98(2)	0.44(9)	$E2$	$23/2^+ \rightarrow 19/2^+$	10
879.5	12	1.20(8)	0.35(10)	$E2$	$39/2^+ \rightarrow 35/2^+$	10
978.0	12	0.95(6)	0.41(11)	$E2$	$43/2^+ \rightarrow 39/2^+$	10
988	<1				$(51/2^+ \rightarrow 47/2^+)$	9
1064.5	11	1.13(9)	0.21(11)	$E2$	$47/2^+ \rightarrow 43/2^+$	10
1087	<1				$(55/2^+ \rightarrow 51/2^+)$	9
1146.0	11	1.00(8)	0.26(10)	$E2$	$51/2^+ \rightarrow 47/2^+$	10
1175.5	3.0				$59/2^+ \rightarrow (55/2^+)$	9
1228.6	10	1.11(9)	0.37(12)	$E2$	$55/2^+ \rightarrow 51/2^+$	10
1265.1	9.8	0.92(9)		$E2$	$63/2^+ \rightarrow 59/2^+$	9
1301.3	9.9	0.95(9)		$E2$	$59/2^+ \rightarrow 55/2^+$	9$\rightarrow$10
1356	<1				$(55/2^+) \rightarrow 51/2^+$	9$\rightarrow$10
1356.8	9.0				$(67/2^+) \rightarrow 63/2^+$	9
1495.4	8.7				$(71/2^+ \rightarrow 67/2^+)$	9
1636	8.2				$(75/2^+ \rightarrow 71/2^+)$	9
1765	7.2				$(79/2^+ \rightarrow 75/2^+)$	9
1903	4.1				$(83/2^+ \rightarrow 79/2^+)$	9

Bands 11–14

E_γ (keV) [a]	I_γ [b]	R_Q	P	Mult.	Assignment	Band
103.5	2.1				$11/2^- \rightarrow 9/2^+$	12$\rightarrow$8
337.1	125	0.96(1)	0.15(2)	$E2$	$15/2^- \rightarrow 11/2^-$	12
447.7	8	0.95(3)		$E2$	$15/2^- \rightarrow 11/2^-$	14
470.2	118	1.01(1)	0.32(2)	$E2$	$19/2^- \rightarrow 15/2^-$	12
479.2	4.9				$11/2^- \rightarrow (9/2^+)$	14$\rightarrow$
485.1	12	0.99(2)		$E2$	$19/2^- \rightarrow 15/2^-$	14
495.9	<1	0.91(4)		$M1/E2$	$11/2^- \rightarrow 11/2^-$	14$\rightarrow$12
512	3.0	0.80(3)		$E1$	$11/2^- \rightarrow 9/2^+$	14$\rightarrow$
535	<1				$27/2^- \rightarrow 27/2^-$	14$\rightarrow$12
535.5	18	0.98(2)		$E2$	$23/2^- \rightarrow 19/2^-$	14
553	<1				$23/2^- \rightarrow 23/2^-$	14$\rightarrow$12
602.9	$\equiv 100$	1.01(1)	0.31(2)	$E2$	$23/2^- \rightarrow 19/2^-$	12
603	0.5				$(9/2^+) \rightarrow 7/2^+$	$\rightarrow$10
607.0	35	1.09(2)		$E2$	$43/2^- \rightarrow 39/2^-$	13
607.3	4.5				$15/2^- \rightarrow 15/2^-$	14$\rightarrow$12
619.4	1.5				$11/2^- \rightarrow 7/2^+$	12$\rightarrow$10
620	<1				$19/2^- \rightarrow 19/2^-$	14$\rightarrow$12
637	0.2				$(9/2^+) \rightarrow 7/2^+$	$\rightarrow$10
647.3	2.5	1.06(3)		$E2$	$43/2^- \rightarrow 39/2^-$	13$\rightarrow$12
661.3	3.0	0.96(3)		$E2$	$9/2^+ \rightarrow 5/2^+$	$\rightarrow$8
694.7	5.1				$(9/2^+) \rightarrow 5/2^+$	$\rightarrow$8
699.5	20	0.98(2)		$E2$	$31/2^- \rightarrow 27/2^-$	14
713	<1				$47/2^- \rightarrow 43/2^-$	13$\rightarrow$12
713.1	20	1.04(2)		$E2$	$27/2^- \rightarrow 23/2^-$	14
731.6	94	0.99(1)	0.25(2)	$E2$	$27/2^- \rightarrow 23/2^-$	12
757.5	6.1					$\rightarrow$13
759.1	17	0.96(2)		$E2$	$35/2^- \rightarrow 31/2^-$	14
812.1	1.1	0.92(4)		$E2$	$39/2^- \rightarrow 35/2^-$	12$\rightarrow$14
841.0	88	1.01(1)	0.33(2)	$E2$	$31/2^- \rightarrow 27/2^-$	12
853.1	16	1.03(2)	0.41(6)	$E2$	$39/2^- \rightarrow 35/2^-$	13$\rightarrow$14

TABLE I (*Continued.*)

E_γ (keV) [a]	I_γ [b]	R_D	P	Mult.	Assignment	Band
941.3	82	1.04(1)	0.47(3)	$E2$	$35/2^- \rightarrow 31/2^-$	12
955.1	<1				$(39/2^-) \rightarrow 35/2^-$	14
968.0	4.1	0.96(4)		$E2$	$43/2^- \rightarrow 39/2^-$	$12 \rightarrow 13$
996.0	1.4				$\rightarrow 47/2^-$	$\rightarrow 13$
1008.5	48	1.09(3)	0.27(7)	$E2$	$43/2^- \rightarrow 39/2^-$	12
1014.3	10	1.00(3)		$E2$	$51/2^- \rightarrow 47/2^-$	13
1021.3	3.0				$\rightarrow 51/2^-$	13
1025.0	61	1.01(2)	0.37(5)	$E2$	$39/2^- \rightarrow 35/2^-$	12
1045.3	42	1.04(3)	0.51(8)	$E2$	$47/2^- \rightarrow 43/2^-$	12
1065.7	18	1.01(2)	0.38(10)	$E2$	$39/2^- \rightarrow 35/2^-$	$13 \rightarrow 12$
1074.5	19	1.07(3)	0.61(10)	$E2$	$47/2^- \rightarrow 43/2^-$	13
1081.3	8.1				$(63/2^-) \rightarrow 59/2^-$	12
1084.4	1.6				$43/2^- \rightarrow 39/2^-$	$11 \rightarrow 13$
1091.6	3.1	1.10(5)		$E2$	$19/2^- \rightarrow 15/2^-$	$14 \rightarrow 12$
1125.0	30	0.98(3) [c]	0.42(8) [c]	$E2$	$51/2^- \rightarrow 47/2^-$	12
1125.4	4.1	0.98(3) [c]	0.42(8) [c]	$E2$	$43/2^- \rightarrow 39/2^-$	$11 \rightarrow 12$
1131	<1				$(63/2^-) \rightarrow 59/2^-$	$12 \rightarrow$
1140.0	5.0	1.37(10)		$E2$	$47/2^- \rightarrow 43/2^-$	11
1155.9	16.8	0.89(5)	0.29(9)	$E2$	$59/2^- \rightarrow 55/2^-$	$\rightarrow 11$
1156.7	5.1				$23/2^- \rightarrow 19/2^-$	$14 \rightarrow 12$
1156.9	2.4					
1176	1.6					
1178	6.4 [c]	1.08(6) [c]		$E2$	$55/2^- \rightarrow 51/2^-$	$12 \rightarrow$
1179	6.4 [c]	1.08(6) [c]		$E2$	$51/2^- \rightarrow 47/2^-$	$\rightarrow 11$
1191.8	4.6				$(51/2^-) \rightarrow 47/2^-$	11
1195.9	4.0				$(67/2^- \rightarrow 63/2^-)$	12
1206.6	15	1.10(7)		$E2$	$59/2^- \rightarrow 55/2^-$	12
1217	2.5				$55/2^- \rightarrow 51/2^-$	11
1233.1	23	0.98(4)	0.64(11)	$E2$	$55/2^- \rightarrow 51/2^-$	12
1255.5	2.4				$47/2^- \rightarrow 43/2^-$	$11 \rightarrow 12$
1267	<1				$27/2^- \rightarrow 23/2^-$	$14 \rightarrow 12$
1297.2	1.8				$59/2^- \rightarrow 55/2^-$	11
1407.2	4.1	1.05(8)		$E2$	$47/2^- \rightarrow 43/2^-$	$12 \rightarrow 13$
1457.2	<1	0.97(7)		$E2$	$51/2^- \rightarrow 47/2^-$	$12 \rightarrow 13$
1593	<1				$55/2^- \rightarrow 51/2^-$	$12 \rightarrow 13$

[a] γ-ray energies are accurate to ± 0.3 keV for the strong transitions ($I_\gamma > 10$) rising to ± 0.6 keV for the weaker transitions. Energies quoted as integers have errors ± 1 keV.

[b] Errors on the relative intensities are estimated to be less than 5% of the quoted values for strong transitions ($I_\gamma > 10$) and less than 10% for the weaker transitions.

[c] Value given for doublet peak.

polarization matrices. The resulting spectrum of Fig. 4(a) has been gated by transitions from ^{117}I, while the spectrum of Fig. 4(b) used the total projections. A positive difference is expected for electric transitions while a negative difference is expected for magnetic transitions. In addition to the discrete peaks of Fig. 4(b), an unresolved $M1$ continuum (negative hump) is seen centered around energies of 400 keV. A corresponding $E2$ continuum (positive background) is seen above energies of 700 keV. The former $M1$ continuum corresponds to the intense $\Delta I = 1$ transitions of strongly coupled configurations, while the latter $E2$ continuum corresponds to the collective $\Delta I = 2$ transitions of rotational bands.

The experimental linear-polarization results for ^{117}I are included in Table I, while the results for bands 3 (magnetic dipole) and 12 (electric quadrupole) are shown in Fig. 5. For transitions below 200 keV, the small probability of Compton scattering between clover elements precluded a polarization measurement. The experimental values average around $P \approx 0.40$ for stretched $E2$ transitions, and $P \approx -0.20$ for mixed $M1/E2$ dipole transitions.

C. Band structures in ^{117}I

The γ-rays assigned to ^{117}I have been arranged into several band structures in Fig. 1 in order to facilitate the discussion. Bands 1–5 consist of strongly coupled structures with strong $\Delta I = 1$ transitions relative to the $E2$ crossovers. Bands 6–14 consist of $\Delta I = 2$ structures.

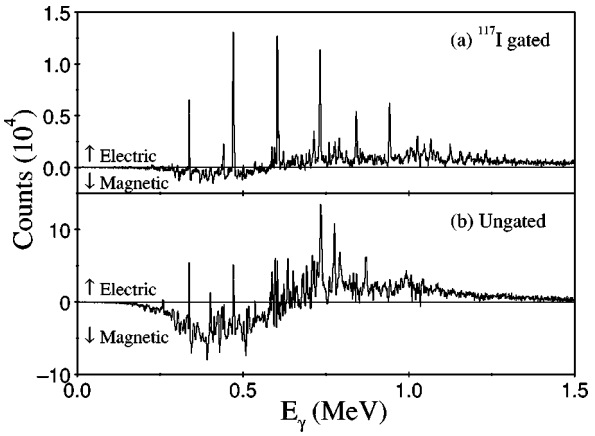

FIG. 4. Spectra of clover perpendicular scatters (with respect to the reaction plane) minus parallel scatters. Positive peaks correspond to electric transitions, negative peaks to magnetic transitions. Spectrum (a) has been gated by the strong low-lying transitions of band 12.

1. The strongly coupled bands

Bands 1–4 are shown in Fig. 1(a), where it can be seen that bands 1, 2, and 4 decay into band 3 which subsequently decays into the lowest levels of bands 8 and 10. The strongly coupled band 5 is included in Fig. 1(b) and, in addition to decaying to band 3 (the lowest states of this band are included in this figure), several links have been established into bands 8, 10, 12, and 14, respectively.

Band 3 is based on a $\pi g_{9/2}^{-1}$ orbital, common in this mass region, with a bandhead spin and parity $I^\pi = 9/2^+$. The loss of coincident intensity across the $9/2^+$ bandhead is consistent with the known lifetime of 17.5 ns for this state [15]. The band has been extended to $I^\pi = (53/2^+)$ through a backbend at $I \sim 29/2$; the extension to high spin was hampered by the observation of several doublet and triplet (both $\Delta I = 1$ and $\Delta I = 2$) transitions. It was only with the power of a γ^4 analysis that these γ-rays could be placed in the band structure with some certainty. Furthermore, the higher $E2$ transitions of this band were only discernible in a 1D spectrum triple gated by all the strong $\Delta I = 1$ transitions; this spectrum is shown in Fig. 2(b).

Band 2 decays into band 3 via a 628 keV linking transition. The measured R_D value for this link is consistent with $\Delta I = 1$ character, although $\Delta I = 2$ character was tentatively assigned in Ref. [2]. Loss of coincident intensity across the $19/2^{(-)}$ bandhead implies a lifetime of a few nanoseconds. Negative parity for this band is deduced from measured $B(M1)/B(E2)$ ratios (see Sec. IV B). Again, the higher $E2$ members of this band could only be identified in a spectrum triple gated by all the strong $\Delta I = 1$ transitions; this spectrum is shown in Fig. 2(a).

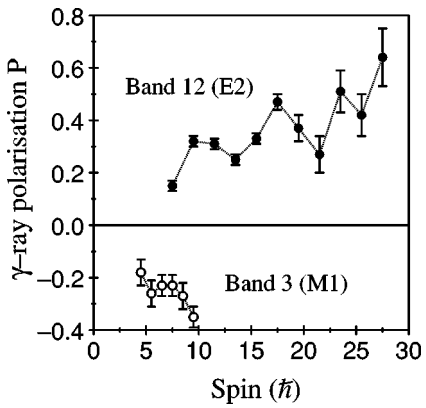

FIG. 5. Experimental linear polarizations extracted for band 3 and band 12.

The lowest members of band 1, in addition to the linking 688 keV and 988 keV transitions into band 3, were observed in Ref. [2] and a bandhead spin and parity $I^\pi = 11/2^-$ suggested. However, in the present data, the observation of the 206 keV transition linking bands 2 and 1, with an R_D value consistent with $\Delta I = 1$ character, rather suggests a bandhead spin of 13/2 for band 1. A similar structure has been observed in ^{119}I with positive parity [30] and hence we now tentatively assign positive parity to band 1.

Band 4 is newly identified and the angular correlation results suggest positive parity. The higher part of band 5 was identified in Ref. [2], where significant decay was observed through the $25/2^+$ state X of Fig. 1(b). Decay of level X back into band 5 is observed, and a similar situation occurs for the newly identified level Y $(27/2^+)$ of Fig. 1(b). Band 5 has been followed to lower spin and new decay paths established. The angular correlation results suggest positive parity for this band.

2. The decoupled bands

The strongly populated (yrast) band 12 is based on a $\pi h_{11/2}$ intruder orbital, common in this mass region. The excitation energy of the bandhead (678 keV) was inferred in Ref. [2] through the observation of several transitions decaying ultimately into the $5/2^+$ ground state, and is confirmed by the present data. The weak coincident intensity observed across the $11/2^-$ bandhead suggests that this state is isomeric with a lifetime of the order of tens of nanoseconds. The partial lifetime for the 619 keV $11/2^- \rightarrow 7/2^+$ $M2$ decay is consistent with single-particle estimates for such decay. Band 12 has been extended to $I^\pi = (67/2^-)$ but no further transitions could be placed above this state despite the strong population intensity.

Bands 13 and 14 were previously observed in Ref. [2]. In the previous work, the 1075 keV and 1015 keV transitions of band 13 were assigned as $\Delta I = 1$ transitions. However, the present angular correlation analysis clearly shows that these transitions are stretched $E2$ transitions; the observation of the high energy transitions (1406, 1457, and 1593 keV) linking bands 12 and 13 confirm the present assignment. Band 11 is newly identified and feeds band 12 via a 1125 keV transition. Note that another 1125 keV transition is placed in band 12.

Bands 6 and 7 were previously observed in Ref. [2] but only tentative spin and parity assignments were available. The present spin and parity assignments follow from the angular correlation analysis. The three transitions linking bands 6 and 7 are consisitent with stretched $E2$ character rather than dipole character as suggested in Ref. [2]. A new self-coincident doublet (430 keV) is placed between the $55/2^+$ level of band 7 and the $51/2^+$ level of band 6. This defines a new state at $53/2^+$. Two dipole transitions (915 and 948 keV) with very low R_Q values, i.e., negative $M1/E2$ multi-

pole mixing ratios, feed the two highest states of band 7.

Bands 9 and 10 are newly identified, although the lowest four γ-rays of band 10 were tentatively placed in Ref. [2]. Band 10 is followed to $I^{\pi}=55/2^{+}$ through the angular correlation analysis, while band 9 is observed to $I^{\pi}=(83/2^{+})$; note that band 9 is observed to much higher spin and excitation energy than any of the other bands in ^{117}I.

IV. DISCUSSION

A. Low-spin band assignments

Similar to heavier odd-Z iodine isotopes, the ground state of ^{117}I has been assigned $I^{\pi}=5/2^{(+)}$ [31]. Magnetic moment measurements are consistent with predominantly $d_{5/2}$ character. In terms of Nilsson assignments, band 8 represents the rotational band built on the favored signature component ($\alpha=+1/2$) of the $[420]1/2^{+}(\pi d_{5/2})$ configuration. Band 10, based on a $7/2^{+}$ state just 58 keV above the ground state, may be associated with the favoured signature component ($\alpha=-1/2$) of the $[422]3/2^{+}$ $(\pi g_{7/2})$ orbital. Band 3, 353 keV above the ground state, represents a strongly coupled band based on the $[404]9/2^{+}$ $(\pi g_{9/2}^{-1})$ Nilsson state; such bands are a common feature of odd-A iodine isotopes. Similarly, the strongly populated (yrast) band 12, 678 keV above the ground state, represents the rotational band built on the favored ($\alpha=-1/2$) signature component of the $[550]1/2^{-}$ $(\pi h_{11/2})$ intruder orbital.

Several strongly coupled bands (1–5) are evident in ^{117}I. In addition to placing the odd proton in the high-Ω $[404]9/2^{+}$ Nilsson orbital, strongly coupled bands can also be constructed by forming high-K 2-quasineutron states, namely $\{[402]5/2^{+}\otimes[532]5/2^{-}\}_{K^{\pi}=5^{-}}(\nu d_{5/2}h_{11/2})$ and $\{[413]5/2^{+}\otimes[532]5/2^{-}\}_{K^{\pi}=5^{-}}(\nu g_{7/2}h_{11/2})$ configurations, and coupling these to the available odd proton orbitals. These high-Ω neutron orbitals are known to form the low-spin structures in neighboring odd-N ^{117,119}Xe [26,32]. Specific configuration assignments are discussed in Sec. IV B. Band 14, with the same spins and parity as band 12, has previously been assigned as the band 12 configuration $(\pi h_{11/2})$ coupled to the γ-vibration of the core [2]. Similarly, with the new (tentative) spin and parity assignments of band 1, it seems plausible to associate this band with the $\pi g_{9/2}^{-1}$ state coupled to the γ-vibration of the core, as suggested for the corresponding band in ^{119}I [30].

B. $B(M1)/B(E2)$ ratios

$B(M1;I\rightarrow I-1)/B(E2;I\rightarrow I-2)$ ratios of reduced transition probabilities may be readily extracted from experimental γ-ray branching ratios of competing $\Delta I=1$ and $\Delta I=2$ transitions and are extremely useful in assigning band configurations. Such ratios have been extracted for the strongly coupled bands and are shown in Fig. 6. Spectra were produced by double gating above the level of interest and measuring the branching ratio of the competing dipole and quadrupole transitions depopulating that level. The dipoles were assumed to be pure magnetic in character with no $E2$ admixture ($\delta\equiv 0$); the $B(M1)/B(E2)$ ratios are not very sensitive to δ since typically $\delta^{2}\ll 1$. Calculated $B(M1)/B(E2)$ ratios are also shown in Fig. 6, using the semiclassical formalism outlined in Refs. [33,34]. In order to perform these calculations, the g-factors of the constituent particles were determined as prescribed in Ref. [35] and the alignments, i_x, and Ω-values of the orbitals estimated from their Nilsson assignments. A quadrupole deformation $\beta_2=0.25$ was assumed, consistent with Woods-Saxon calculations presented in Ref. [3].

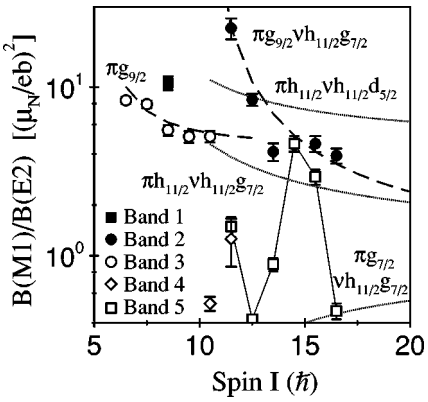

FIG. 6. Experimental $B(M1;I\rightarrow I-1)/B(E2;I\rightarrow I-2)$ ratios of reduced transition probabilities for the strongly coupled bands. Theoretical estimates are also shown by the dotted and dashed lines.

Excellent agreement is found in Fig. 6 between the lower members of band 3 and its expected $\pi g_{9/2}[404]9/2^{+}$ assignment. Due to the number of overlapping doublet and triplet transitions, it was not possible to extract $B(M1)/B(E2)$ ratios for the higher members of this band. The results for band 2 show a sharp rise for the lowest levels. Of the 3-quasiparticle calculations shown in Fig. 6, only the $\pi g_{9/2}\otimes\nu g_{7/2}h_{11/2}$ configuration can reproduce this sharp increase at low spin. Hence we associate this structure with band 2, which suggests negative parity for this band. This specific configuration is built on three high-Ω orbitals, namely the $\{\pi[404]9/2^{+}\otimes\nu[413]5/2^{+}[532]5/2^{-}\}_{K^{\pi}=19/2^{-}}$ configuration with $I=K$ at the bandhead.

Configurations for bands 4 and 5 are not so easy to assign. The measured $B(M1)/B(E2)$ ratios for band 5 show an interesting increase around $I\sim 15$ (see Fig. 6). This occurs at the same spin regime as the levels X and Y in Fig. 1(b). In particular, level X is strongly fed by band 5 and is yrast with respect to the inband $25/2^{+}$ state, as is level Y. These levels are later interpreted as noncollective aligned states (see Sec. IV D). The close proximity of these states to the inband states of band 5, with the same spins and parity, would imply significant mixing of these ''noncollective'' states with the ''collective'' states of band 5. This would reduce the collectivity of the states in band 5 and increase the inband $B(M1)/B(E2)$ values. Therefore, the peak in the $B(M1)/B(E2)$ values for band 5 may be associated with a decrease in collectivity [$B(E2)$ rate] rather than a change in single-particle structure [$B(M1)$ rate]. Furthermore, since the noncollective oblate states all have the odd proton in an $h_{11/2}$ orbital (see Sec. IV D), a likely configuration for strongly coupled band 5 is $\pi h_{11/2}\otimes\nu g_{7/2}h_{11/2}$ (or $\pi h_{11/2}\otimes\nu d_{5/2}h_{11/2}$). The predicted $B(M1)/B(E2)$ ratios of Fig. 6 are however at variance with this interpretation.

C. Quasiparticle alignments

Several of the bands in ^{117}I show evidence for quasiparticle pair alignments, or backbends. Therefore, in order to discuss these effects, the experimental alignment [36],

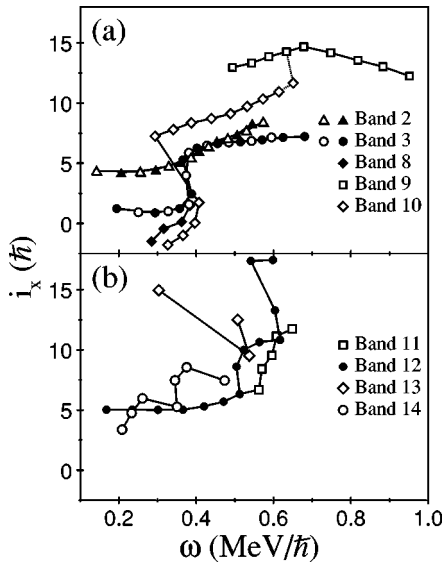

FIG. 7. Experimental alignment, i_x, for some of the bands in ^{117}I plotted as a function of rotational frequency.

$$i_x(\omega) = I_x(\omega) - I_{x,\mathrm{ref}}(\omega), \tag{3}$$

for several of the bands is shown as a function of rotational frequency, ω, in Fig. 7. At a given spin, $I_x(I) = \sqrt{I(I+1)-K^2}$ and $\omega(I) \approx E_\gamma/2\hbar$, while the rotational reference, $I_{x,\mathrm{ref}}$, is given by

$$I_{x,\mathrm{ref}}(\omega) = \omega(\mathcal{J}_0 + \mathcal{J}_1\omega^2) - i_0. \tag{4}$$

Harris parameters [37] $\mathcal{J}_0 = 29.4\hbar^2$ MeV^{-1} and $\mathcal{J}_1 = 4.4\hbar^4$ MeV^{-3} have been used together with $i_0 = 3\hbar$, and provide a reasonable reference over the whole frequency range. These values were obtained from a fit to the lowest five levels of band 12.

Upbends are apparent in bands 3, 8, and 10 (the $[404]9/2^+$, $[420]1/2^+$, and $[422]3/2^+$ bands) at $\omega \sim 0.39$ MeV/$\hbar$ but not the $[550]1/2^-$ intruder band 12 at this frequency. However, an upbend does occur in band 12 at the much higher frequency $\omega \sim 0.50$ MeV/$\hbar$. The upbend is delayed by $\Delta\omega \sim 0.11$ MeV/$\hbar$ in band 12 and this feature has been discussed previously in Refs. [17,19]. Band 3 has been extended through the backbend and gains $\approx 6\hbar$ of alignment. This is similar to the gain of alignment for the delayed backbend in band 12 and is attributed to the rotational alignment of a pair of $h_{11/2}$ neutrons in the $[532]5/2^-$ Nilsson state. Band 10 shows a sharp backbend at $\omega \sim 0.39$ MeV/$\hbar$ with a larger gain in alignment of $\approx 8\hbar$. A similar situation is encountered in the corresponding band of ^{119}I and is again attributed to $h_{11/2}$ neutron alignment [30]. A second backbend is seen in band 12 above $\omega = 0.60$ MeV/$\hbar$. Such a sharp backbend is not expected for a normal quasiparticle pair alignment, and may instead imply a transition to a noncollective regime.

D. High-spin properties

In this section, the high-spin properties of ^{117}I are discussed with regard to band termination. The $39/2^-$ and (yrast) $43/2^-$ states of band 13 have previously been interpreted as specific noncollective oblate ($\gamma = 60°$) states based on energetically favorable $\pi[(g_{7/2}/d_{5/2})^2(h_{11/2})^1]_{23/2^-} \otimes \nu[(g_{7/2}/d_{5/2})^{10}(h_{11/2})^4]_{8^+,10^+}$ configurations, respectively, relative to the $N = Z = 50$ doubly magic core [2,17]. Several other theoretical oblate states have been discussed in Ref. [2] (see Fig. 12 of Ref. [2]), where total Routhian surface (TRS) calculations using a Woods-Saxon potential [39–42] have been considered. Some of these configurations are listed in Table II. The states at $25/2^+$ and $27/2^+$, labeled X and Y in Fig. 1(b), could correspond to the noncollective configurations at these spins listed in Table II. All the noncollective states of Table II contain a single $h_{11/2}$ odd proton but no excitations (i.e., $\pi g_{9/2}^{-1,-2}$) across the $Z = 50$ shell gap.

1. Smooth band termination

The energies of the experimental bands are plotted relative to a rigid-rotor reference in Fig. 8 to show the global systematics for the bands. It can be seen in this figure that band 9 shows the characteristic upturn at high spin that is associated with a smoothly terminating band [9]. Expanded, high spin rigid-rotor plots for positive and negative parity are shown in Fig. 9 and Fig. 10, respectively, compared to some theoretical configurations with parity and signature $(\pi,\alpha) = (+,-1/2)$ and $(-,-1/2)$. These calculations, with constrained orbital occupancy, have been performed using the configuration-dependent shell-correction approach with an unpaired, cranked Nilsson potential, as described in Refs. [9,13,14], and using the Nilsson parameter set of Ref. [38]. The calculated configurations are labeled using the $[p_1p_2,n_1(n_2)]$ nomenclature of Ref. [14], i.e., p_1 represents the number of $\pi g_{9/2}$ holes, p_2 represents the number of $\pi h_{11/2}$ particles and n_1 represents the number of $\nu h_{11/2}$ particles, relative to the $Z = N = 50$ doubly magic core. However, compared with Ref. [14], n_2 has been added to indicate the number of $\nu i_{13/2}$ particles. In most configurations, no $\nu i_{13/2}$ particles are present and then n_2 is omitted; however the $[01,3(1)]$ $\nu i_{13/2}$ configuration, which terminates at $I^\pi = 71/2^+$, is drawn in Fig. 9(b). Given that ^{117}I is reasonably far from the $Z = N = 50$ doubly magic core, many single-particle configurations have been considered. The theoretical shape evolution of selected configurations through the $\varepsilon_2 - \gamma$ plane is shown in Fig. 11.

TABLE II. Some theoretical noncollective oblate states in ^{117}I [2] and their experimental candidates.

Configuration	Experimental state
$\pi[(g_{7/2}/d_{5/2})^2(h_{11/2})^1]_{23/2^-} \otimes \nu[(g_{7/2}/d_{5/2})^{10}(h_{11/2})^4]_{8^+}$	$39/2^-$ level of band 13
$\pi[(g_{7/2}/d_{5/2})^2(h_{11/2})^1]_{23/2^-} \otimes \nu[(g_{7/2}/d_{5/2})^{10}(h_{11/2})^4]_{10^+}$	$43/2^-$ level of band 13
$\pi[(g_{7/2}/d_{5/2})^2(h_{11/2})^1]_{11/2^-} \otimes \nu[(g_{7/2}/d_{5/2})^{11}(h_{11/2})^3]_{7^-}$	$25/2^+$ level X
$\pi[(g_{7/2}/d_{5/2})^2(h_{11/2})^1]_{11/2^-} \otimes \nu[(g_{7/2}/d_{5/2})^{11}(h_{11/2})^3]_{8^-}$	$27/2^+$ level Y

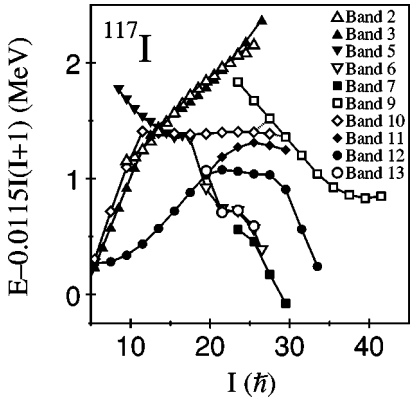

FIG. 8. The energies of the experimental bands in ^{117}I shown relative to a rigid-rotor reference.

For band 9, the best theoretical agreement is found for either the [12,4] configuration or for the $[22,4]_1$ configuration. The former configuration, containing one $\pi g_{9/2}$ proton hole, would be expected to generate a strongly coupled band with two degenerate signature components connected by strong dipole transitions (cf. bands 2 and 3). Since no evidence for a signature partner band has been found, it seems reasonable to exclude this configuration. The minimum in the theoretical rigid-rotor plot for the $[22,4]_1$ configuration matches well the experimental minimum for band 9 (see Fig. 9). The $[22,4]_1$ configuration ultimately terminates beyond $I=50\hbar$, several units of spin higher than seen experimentally in band 9. A problem with this configuration is, however, that its signature partner is calculated a few hundred keV lower in energy and then it is difficult to understand why this signature partner band has not also been observed. Above spin 40, the $[22,4]_2$ configuration becomes yrast. In this configuration, the ten positive-parity neutrons are rearranged amongst the available $N=4$ orbitals; specifically, the lowest

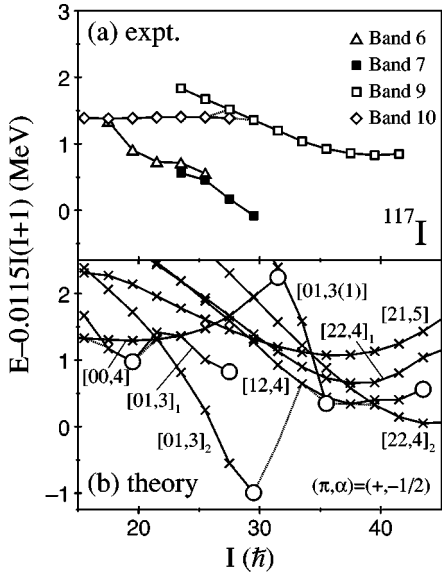

FIG. 9. The energies of the positive-parity experimental bands in ^{117}I at high spin (a), and selected theoretical configurations (b), shown relative to a rigid-rotor reference. The open circles in (b) represent oblate terminating states, while the dotted line follows the locus of theoretical yrast states.

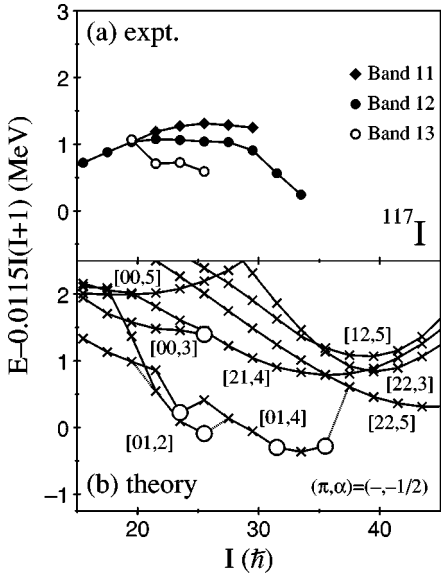

FIG. 10. Same as Fig. 9 but for negative parity.

$\nu d_{3/2}$ orbital becomes occupied. This band is the favored signature branch; however, the minimum in the rigid-rotor plot is at a much higher spin value than for the experimental band 9. Thus, we have not found any calculated configuration which explains the observed band 9 in a natural way, but prefer the $[22,4]_1$ interpretation. Band 9 crosses band 10 at approximately the same spin that the $[22,4]_1$ configuration crosses the [00,4] configuration. Therefore, this latter configuration may be associated with band 10 and is consistent with its quasiparticle interpretation, namely a $\pi g_{7/2} \otimes [\nu h_{11/2}]^2$ three-quasiparticle configuration at high spin (note that only the aligned quasiparticles are labeled here).

Bands 6 and 7 are strongly yrast in the spin region $I \approx 18-30\hbar$ and are best described by configurations of the form [01,3]. These configurations are unstable with large triaxial shapes even at low spin, as shown in Fig. 11. Oblate shapes are found for $I^\pi = 39/2^+$, $55/2^+$, and $59/2^+$, which may be identified with states in bands 6 and 7. Note that the topmost transition of band 7 with $I^\pi = 59/2^+$ matches the highest spin available for the $[01,3]_2$ configuration, with a

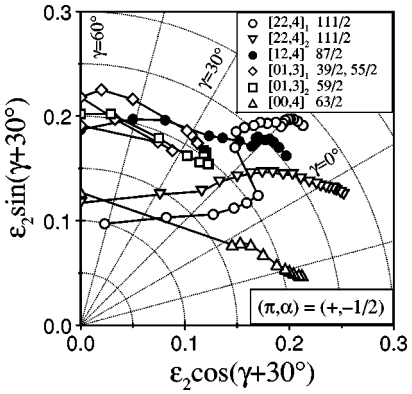

FIG. 11. Theoretical evolution of the nuclear shape for some $(\pi,\alpha)=(+,-1/2)$ configurations in ^{117}I. The data points are separated by $2\hbar$ and the terminating spins (at $\gamma=60°$) are given in the top inset.

terminating configuration $\pi[(g_{7/2}/d_{5/2})^2_6(h_{11/2})^1_{11/2}] \otimes \nu[(g_{7/2}/d_{5/2})^{-3}_{9/2}(h_{11/2})^3_{27/2}]$ relative to a ^{114}Sn core. The three neutron holes do not couple to their maximum spin of 17/2 but instead to 9/2, which is caused by the relatively large (oblate) deformation ($\varepsilon_2 \approx 0.2$) at termination. Despite the intensity of band 7, no further ($E2$) transitions could be observed extending the band to higher spin. This is consisitent with the calculations which show a large rise in energy [Fig. 9(b)] for spins beyond 59/2. In essence, decay from higher spin states proceeds via the $[22,4]_1$ and [00,4] configurations, namely bands 9 and 10, and bypasses the strongly yrast $[01,3]_2$ states with $I = 20-30\hbar$.

No experimental evidence has been found for negative-parity terminating bands at high spin. The lowest-energy theoretical terminating configuration that could give rise to a long band structure at intermediate spin is the [21,4] configuration, as shown in Fig. 10(b). Above spin $35\hbar$, the [22,5] configuration becomes yrast. However, these configurations are predicted to lie $\sim$1.5 MeV above [01,4] and [01,2] configurations for spins $20-35\hbar$. Indeed, the $(\pi, \alpha) = (-, -1/2)$ yrast line for spins $15-35\hbar$ consists of these [01,2] and [01,4] configurations. Similar to the positive-parity $[01,3]_{1,2}$ configurations, these configurations appear unstable with respect to γ; for instance three oblate states occur at $I^\pi = 47/2^-$, $63/2^-$, and $71/2^-$ for the [01,4] configuration. The $47/2^-$ oblate state, together with the $51/2^-$ oblate state of the [01,2] configuration could be associated with the higher members of band 13. The $39/2^-$ and $43/2^-$ states of band 13 have already been identified with noncollective oblate states [2]. Similar to the positive-parity configurations, generation of spin beyond $71/2^-$ is energetically expensive, which again explains why the strong yrast band 12 could not be extended to higher spin than shown in Fig. 1.

V. CONCLUSIONS

High-spin states have been investigated in ^{117}I using the EUROGAM II γ-ray spectrometer and the level scheme has been significantly extended through a high-fold (4D) analysis. Although the ^{31}P+^{90}Zr reaction produced many open channels, a high-fold analysis has provided a wealth of new information. Indeed, well over one thousand discrete γ-ray transitions have been placed in over a dozen nuclei from this data set, illustrating the immense resolving power of the new generation of high-efficiency multidetector γ-ray spectrometers. In particular, over 250 γ-rays have been assigned to ^{117}I and the level scheme significantly extended.

In addition to specific aligned noncollective oblate states in ^{117}I, evidence has been found for a positive-parity high-spin band which has been linked into the low-spin level scheme. This band may be assigned a [22,4] configuration, i.e., a configuration involving a $\pi(g_{9/2})^{-2}(h_{11/2})^2$ 2-particle–2-hole excitation across the $Z = 50$ shell gap.

ACKNOWLEDGMENTS

The EUROGAM project is jointly funded by the EPSRC (UK) and IN2P3 (France). This work was also partly funded by grants from the National Science Foundation (USA) and by the Swedish Natural Science Research Council. I.R. is grateful for financial support from the Crafoord Foundation (Lund, Sweden) and the Royal Swedish Academy of Sciences. A.N.W. and J.N.W. acknowledge receipt of EPSRC support during the course of this work, while K.H. acknowledges financial support from the University of York. Finally, the authors are indebted to Dr. D.C. Radford for providing the RADWARE analysis codes.

[1] E.S. Paul, R.M. Clark, S.A. Forbes, D.B. Fossan, J.R. Hughes, D.R. LaFosse, Y. Liang, R. Ma, P.J. Nolan, P.H. Regan, P. Vaska, R. Wadsworth, and M.P. Waring, J. Phys. G **18**, 837 (1992).

[2] M.P. Waring, D.B. Fossan, J.R. Hughes, D.R. LaFosse, Y. Liang, R. Ma, P. Vaska, S.A. Forbes, E.S. Paul, R.M. Clark, and R. Wadsworth, Phys. Rev. C **48**, 2629 (1993).

[3] Y. Liang, D.B. Fossan, J.R. Hughes, D.R. LaFosse, T. Lauritsen, R. Ma, E.S. Paul, M.P. Waring, P. Vaska, and N. Xu, Phys. Rev. C **45**, 1041 (1992).

[4] Y. Liang, D.B. Fossan, J.R. Hughes, D.R. LaFosse, T. Lauritsen, R. Ma, E.S. Paul, P. Vaska, M.P. Waring, N. Xu, and R.A. Wyss, Phys. Rev. C **44**, R578 (1991).

[5] D.L. Balabanski, G. Rainovski, N. Blasi, G. Falconi, G. Lo Bianco, S. Signorelli, D. Bazzacco, G. de Angelis, D.R. Napoli, M.A. Cardona, A.J. Kreiner, and H. Somacal, Phys. Rev. C **56**, 1629 (1997).

[6] D.M. Gordon, M. Gai, A.K. Gaigalas, R.E. Shroy, and D.B. Fossan, Phys. Lett. **67B**, 161 (1977).

[7] J. Bron, W.H.A. Hesselink, A. van Poelgeest, J.J.A. Zalmstra, M.J. Uitzinger, H. Verheul, K. Heyde, M. Waroquier, H. Vincx, and P. van Isacker, Nucl. Phys. **A318**, 335 (1979).

[8] V.P. Janzen, D.R. LaFosse, H. Schnare, D.B. Fossan, A. Galindo-Uribarri, J.R. Hughes, S.M. Mullins, E.S. Paul, L. Persson, S. Pilotte, D.C. Radford, I. Ragnarsson, P. Vaska, J.C. Waddington, R. Wadsworth, D. Ward, J.N. Wilson, and R. Wyss, Phys. Rev. Lett. **72**, 1160 (1994).

[9] I. Ragnarsson, V.P. Janzen, D.B. Fossan, N.C. Schmeing, and R. Wadsworth, Phys. Rev. Lett. **74**, 3935 (1995).

[10] R. Wadsworth, R.M. Clark, J.A. Cameron, D.B. Fossan, I.M. Hibbert, V.P. Janzen, R. Krücken, G.J. Lane, I.Y. Lee, A.O. Macchiavelli, C.M. Parry, J.M. Sears, J.F. Smith, A.V. Afanasjev, and I. Ragnarsson, Phys. Rev. Lett. **80**, 1174 (1998).

[11] M.P. Waring, E.S. Paul, C.W. Beausang, R.M. Clark, R.A. Cunningham, T. Davinson, S.A. Forbes, D.B. Fossan, S.J. Gale, A. Gizon, J. Gizon, K. Hauschild, I.M. Hibbert, A.N. James, P.M. Jones, M.J. Joyce, D.R. LaFosse, R.D. Page, I. Ragnarsson, H. Schnare, P.J. Sellin, J. Simpson, P. Vaska, R. Wadsworth, and P.J. Woods, Phys. Rev. C **51**, 2427 (1995).

[12] E.S. Paul, H.R. Andrews, V.P. Janzen, D.C. Radford, D. Ward, T.E. Drake, J. DeGraaf, S. Pilotte, and I. Ragnarsson, Phys. Rev. C **50**, 741 (1994).

[13] T. Bengtsson and I. Ragnarsson, Nucl. Phys. **A436**, 14 (1985).

[14] A.V. Afanasjev and I. Ragnarsson, Nucl. Phys. **A591**, 387 (1995).

[15] M. Gai, D.M. Gordon, R.E. Shroy, and D.B. Fossan, Phys. Rev. C **26**, 1101 (1982).

[16] W.F. Piel, Jr., P. Chowdury, U. Garg, M.A. Quader, P.M. Stwertka, S. Vadja, and D.B. Fossan, Phys. Rev. C **31**, 456 (1985).
[17] E.S. Paul, M.P. Waring, R.M. Clark, S.A. Forbes, D.B. Fossan, J.R. Hughes, D.R. LaFosse, Y. Liang, R. Ma, P. Vaska, and R. Wadsworth, Phys. Rev. C **45**, R2531 (1992).
[18] S. Juutinen, S. Törmänen, P. Ahonen, B. Cederwall, A. Johnson, B. Fant, R. Julin, S. Mitarai, J. Mukai, J. Nyberg, and A. Virtanen, Z. Phys. A **344**, 223 (1992).
[19] E.S. Paul, D.B. Fossan, K. Hauschild, I.M. Hibbert, H. Schnare, J.M. Sears, I. Thorslund, R. Wadsworth, A.N. Wilson, and J.N. Wilson, Phys. Rev. C **51**, R2857 (1995).
[20] C.W. Beausang and J. Simpson, J. Phys. G **22**, 527 (1996).
[21] P.M. Jones, L. Wei, F.A. Beck, P.A. Butler, T. Byrski, G. Duchêne, G. deFrance, F. Hannachi, G.D. Jones, and B. Kharraja, Nucl. Instrum. Methods Phys. Res. A **362**, 556 (1995).
[22] E.S. Paul, D.B. Fossan, K. Hauschild, I.M. Hibbert, H. Schnare, J.M. Sears, I. Thorslund, R. Wadsworth, A.N. Wilson, and J.N. Wilson, J. Phys. G **21**, 995 (1995); **22**, 653 (1996).
[23] J.M. Sears, D.B. Fossan, I. Thorslund, P. Vaska, E.S. Paul, K. Hauschild, I.M. Hibbert, R. Wadsworth, S.M. Mullins, A.V. Afanasjev, and I. Ragnarsson, Phys. Rev. C **55**, 2290 (1997).
[24] J.M. Sears, I. Thorslund, D.B. Fossan, P. Vaska, E.S. Paul, K. Hauschild, I.M. Hibbert, R. Wadsworth, and S.M. Mullins, Phys. Rev. C **57**, 1656 (1998).
[25] G.J. Lane, D.B. Fossan, C.J. Chiara, H. Schnare, J.M. Sears, J.F. Smith, I. Thorslund, P. Vaska, E.S. Paul, A.N. Wilson, J.N. Wilson, K. Hauschild, I.M. Hibbert, R. Wadsworth, A.V. Afanasjev, and I. Ragnarsson, Phys. Rev. C **58**, 127 (1998).
[26] E.S. Paul, H.C. Scraggs, A.J. Boston, D.B. Fossan, K. Hauschild, I.M. Hibbert, P.J. Nolan, H. Schnare, I. Thorslund, R. Wadsworth, A.N. Wilson, and J.N. Wilson, Nucl. Phys. **A644**, 3 (1998).
[27] D.C. Radford, Nucl. Instrum. Methods Phys. Res. A **361**, 297 (1995); **361**, 306 (1995).
[28] C.W. Beausang, D. Prévost, M.H. Bergström, G. deFrance, B. Haas, J.C. Lisle, Ch. Theisen, J. Timár, P.J. Twin, and J.N. Wilson, Nucl. Instrum. Methods Phys. Res. A **364**, 560 (1995).
[29] K.S. Krane, R.M. Steffen, and R.M. Wheeler, Nucl. Data Tables **11**, 351 (1973).
[30] S. Törmänen, S. Juutinen, R. Julin, A. Lampinen, E. Mäkelä, M. Piiparinen, A. Savelius, A. Virtanen, G.B. Hagemann, Ch. Droste, W. Karczmarczyk, T. Morek, J. Srebrny, and K. Starosta, Nucl. Phys. **A613**, 282 (1997).
[31] J. Blachot and G. Marguier, Nucl. Data Sheets **66**, 451 (1992); and references therein.
[32] H.C. Scraggs, E.S. Paul, A.J. Boston, J.F.C. Cocks, D.M. Cullen, K. Helariutta, P.M. Jones, R. Julin, S. Juutinen, H. Kankaanpää, M. Muikku, P.J. Nolan, C.M. Parry, A. Savelius, R. Wadsworth, A.V. Afanasjev, and I. Ragnarsson, Nucl. Phys. **A640**, 337 (1998).
[33] F. Dönau and S. Frauendorf, in *Proceedings of the Conference on High Angular Momentum Properties of Nuclei*, Oak Ridge, 1982, edited by N.R. Johnson (Harwood Academic, New York, 1983), p. 143.
[34] F. Dönau, Nucl. Phys. **A471**, 469 (1987).
[35] S. Frauendorf, Phys. Lett. **100B**, 219 (1981).
[36] R. Bengtsson and S. Frauendorf, Nucl. Phys. **A327**, 139 (1979).
[37] S.M. Harris, Phys. Rev. **138**, B509 (1965).
[38] J.-y. Zhang, N. Xu, D.B. Fossan, Y. Liang, R. Ma, and E.S. Paul, Phys. Rev. C **39**, 714 (1989).
[39] W. Nazarewicz, J. Dudek, R. Bengtsson, T. Bengtsson, and I. Ragnarsson, Nucl. Phys. **A435**, 397 (1985).
[40] W. Nazarewicz, G.A. Leander, and J. Dudek, Nucl. Phys. **A467**, 437 (1987).
[41] R. Wyss, J. Nyberg, A. Johnson, R. Bengtsson, and W. Nazarewicz, Phys. Lett. B **215**, 211 (1988).
[42] W. Nazarewicz, R. Wyss, and A. Johnson, Nucl. Phys. **A503**, 285 (1989).